Available online at www.sciencedirect.com

ScienceDirect

Cognitive Systems Research 59 (2020) 221–230

Cognitive Systems RESEARCH

www.elsevier.com/locate/cogsys

Brain tumor detection using fusion of hand crafted and deep learning features

Tanzila Saba [a], Ahmed Sameh Mohamed [a], Mohammad El-Affendi [a], Javeria Amin [b,c], Muhammad Sharif [c,*]

[a] College of Computer and Information Sciences, Prince Sultan University, Riyadh, Saudi Arabia
[b] Department of Computer Science, University of Wah, Pakistan
[c] Department of Computer Science, COMSATS University Islamabad, Wah Campus, Pakistan

Received 31 December 2018; received in revised form 28 July 2019; accepted 9 September 2019
Available online 18 September 2019

Abstract

The perilous disease in the worldwide now a days is brain tumor. Tumor affects the brain by damaging healthy tissues or intensifying intra cranial pressure. Hence, rapid growth in tumor cells may lead to death. Therefore, early brain tumor diagnosis is a more momentous task that can save patient from adverse effects. In the proposed work, the Grab cut method is applied for accurate segmentation of actual lesion symptoms while Transfer learning model visual geometry group (VGG-19) is fine-tuned to acquire the features which are then concatenated with hand crafted (shape and texture) features through serial based method. These features are optimized through entropy for accurate and fast classification and fused vector is supplied to classifiers. The presented model is tested on top medical image computing and computer-assisted intervention (MICCAI) challenge databases including multimodal brain tumor segmentation (BRATS) 2015, 2016, and 2017 respectively. The testing results with dice similarity coefficient (DSC) achieve 0.99 on BRATS 2015, 1.00 on BRATS 2015 and 0.99 on BRATS 2017 respectively.

Keywords: Gliomas; Local binary pattern; Histogram orientation gradient; Fusion; Convolutional neural networks (CNNs)

1. Introduction

Gliomas are primary type of brain tumors in the grown-ups which originate apparently from the glial cells and infiltrate nearby brain tissues (Amin, Sharif, Yasmin, & Fernandes, 2017; Menze, 2014). Regardless of comprehensive research developments on gliomas patient, the diagnosis process still remains very poor. The mortality rate of this dreadful disease is rapidly increasing. It is grouped into two groups such as high grade glioma (HGG) and low grade glioma (LGG). The survival rate of HGG is approximately 02 years and requires rapid treatment (Thompson, Mills, Coope, O'connor, and Jackson, 2011). The growth rate of LGG is slower and can be prolonged for many years to maximize the survival rate with proper treatment. The more intensive protocols of neuro-imaging are utilized as prior by hand to evaluate the disease progression rate and for successfully selecting its treatment methodology. In clinical practice, imaging results are assessed on the basis of qualitative procedures such as presence of hyper-intense characteristic in T1c magnetic resonance imaging (MRI) (Nida, Sharif, Khan, Yasmin, & Fernandes, 2016; Strangman, 2009). By the replacement of the current evaluations with more accurate detection of subtumoral structures, automatic procedures are applied for brain tumor

* Corresponding author.
E-mail address: sharif@ciitwah.edu.pk (M. Sharif).

https://doi.org/10.1016/j.cogsys.2019.09.007
1389-0417/

detection. The manual brain tumor segmentation with the help of experts shows more variations when gradients intensity among similar structures are obscured or smooth through bias field. Moreover, the tumor structure varies in terms of shape, size and location from each individual patient Amin, Sharif, Raza, & Yasmin, 2018. The effect of mass is induced through tumor growing which may displace the healthy tissues as a result of which the trustworthiness of preceding spatial facts for healthy tissues becomes limited. The multi-sequence MRI may be utilized to map the changes in brain tissues due to induced tumor region (Menze, 2014). However, each sequence of MRI has biologically different information.

Deep learning methods are considered good for segmentation; particularly convolutional neural network (CNN) (Amin, Sharif, Yasmin, & Fernandes, 2018) is adopted for the recognition of patterns. These methods learn features in the form of hierarchy when compared with statistical methods including support vector machine (SVM) (Shah, Sharif, Yasmin, & Fernandes, 2017; Sharif, Khan, Faisal, Yasmin, & Fernandes, 2018; Liaqat et al., 2018; Ansari, Shah, Yasmin, Sharif, & Fernandes, 2018; Naqi, Sharif, Yasmin, & Fernandes, 2018) that are dependent upon hand crafted features (Havaei, 2017). Deep CNN models are applied successfully for the analysis of medical images including retrieval, segmentation and classification (Litjens, 2017). In medical field, immunochromatographic gold strips are analyzed successfully by using deep CNN model (Mahmud, Kaiser, Hussain, & Vassanelli, 2018). Markov random field (MRF) is also used to analyze the brain tumor in MRI (Bauer, Nolte, & Reyes, 2011).

The major contribution of proposed work is: The input images are converted into a single channel. The Grab cut method with morphological operations is applied to segment and refine tumor region more correctly. In the classification phase, deep features (VGG 19) as well as hand crafted features such as local binary pattern (LBP) and histogram orientation gradient (HOG) are extracted and fused in single features vector for distinguishing gliomas and normal images.

2. Related work

Several algorithms are analyzed for the detection of brain tumor; few are elaborated in this section. The supervised method (random forests) are successfully utilized to segment the brain tumor (Geremia et al., 2010). Gaussian mixture model (GMM) is applied for tumor segmentation (Van Leemput, Maes, Vandermeulen, & Suetens, 1999). Morphological/contextual features provide better results for brain tumor detection (Rao, Ledig, Newcombe, Menon, & Rueckert, 2014). MRF is applied for accurately segmenting the lesion region (Mitra, 2014). Deep learning approaches are powerful because in these, highly discriminative features are extracted automatically in the form of hierarchy. These features provide better results on predefined and hand crafted features. The input images are supplied to five layers CNN model for the classification of enhance, non-enhance and core tumor region (Kleesiek et al., 2014). Different patches are extracted from original images and passed to CNN for segmentation of HGG and LGG cases (Pereira, Pinto, Alves, & Silva, 2015). 2D CNN, U-Net method (Dong, Yang, Liu, Mo, & Guo, 2017), CNN (Pereira, Pinto, Alves, & Silva, 2016), Deep neural networks (DNN) (Havaei, 2017), multi-scale 3D CNN (Kamnitsas, 2017), multi-fractal Detrended fluctuation analysis (MFDFA) (Reza, Mays, & Iftekharuddin, 2015), pairwise affinity and super pixel (Wu, Chen, Zhao, & Corso, 2014), hierarchical classification (Bauer et al., 2012), local independent projection-based classification (Huang et al., 2014), extremely randomized trees (Goetz et al., 2014), generative models (Kwon, Shinohara, Akbari, & Davatzikos, 2014), random field (RF) (Tustison, 2015), fully convolutional neural networks (FCNNs) (Zhao et al., 2018) and cascaded CNN (Havaei, Dutil, Pal, Larochelle, & Jodoin, 2015) methods are utilized the detection of brain tumor. Much work is performed in literature but still there is a gap available to achieve better results on all performance metrics. Hence, proposed model has obtained good results in terms of all performance metrics on five challenges datasets. This is because of a novel fused CNN model presented in this work for brain tumor diagnosis accurately. The summary of existing deep learning methods is mentioned in Table 1.

2.1. Comparison of VGG 19 with other transfer learning models

VGG contains 19 convolutional layers and it has uniform architecture. The Alexnet has 3×3 convolutions only but number of filters are trained on 4 GPU that takes 2–3 weeks. It is widely used for feature extraction. ResNet (residual connection) and Google Net (inception modules) have still low computation as compared to VGG model. VGG model is light weight than other transfer learning models (https://medium.com/@sidereal/cnns-architectures-lenet-alexnet-vgg-googlenet-resnet-and-more-666091488df5). Therefore in this work, VGG architecture is used for feature extraction.

3. Proposed methodology

In the proposed approach, Grab cut method is applied to segment the glioma using MRI. Moreover, segmented images are supplied to the proposed deep learning model as shown in Fig. 1. In this technique, deep features vector is obtained after using VGG19 model. Afterwards, hand crafted (shape and texture) features and deep features are concatenated serially.

3.1. Glioma segmentation using Grab cut method

Initially, RGB image is converted into a single channel. Then Grab cut method is applied for gliomas segmenta-

Table 1
Deep learning methods.

Ref	Year	DL methods	BRATS Datasets	Performance measures (DSC)		
				Complete	Core/non-enhance	Enhance
Zikic, Ioannou, Brown, and Criminisi (2014)	2014	CNN	2013	83.7 ± 9.4	73.6 ± 25.6	69.0 ± 24.9
Dvořák and Menze (2015)	2015	CNN	2014	81 ± 15	79 ± 13	81 ± 11
Pereira et al. (2016)	2016	CNN	2013	0.88	0.83	0.77
Havaei (2017)	2017	DNN	2013	0.81	0.72	0.58
Dong et al. (2017)	2017	U-Net CNN	2015	0.86	0.86	0.65
Kamnitsas (2017)	2017	3D-CNN + RF	2015	0.84	0.66	0.63
Zhao et al. (2018)	2018	FCNN model	2013	0.70	0.62	0.64
Abd-Ellah, Awad, Khalaf, and Hamed (2018)	2018	CNN	2013	0.87	–	–
Hussain, Anwar, and Majid (2018)	2018	DNN	2013	0.87	0.89	0.92
			2015	0.86	0.87	0.90
Chen, Ding, and Liu (2019)	2019	Dual-force CNN	2015	0.85	0.70	0.63
			2017	0.89	0.73	0.73

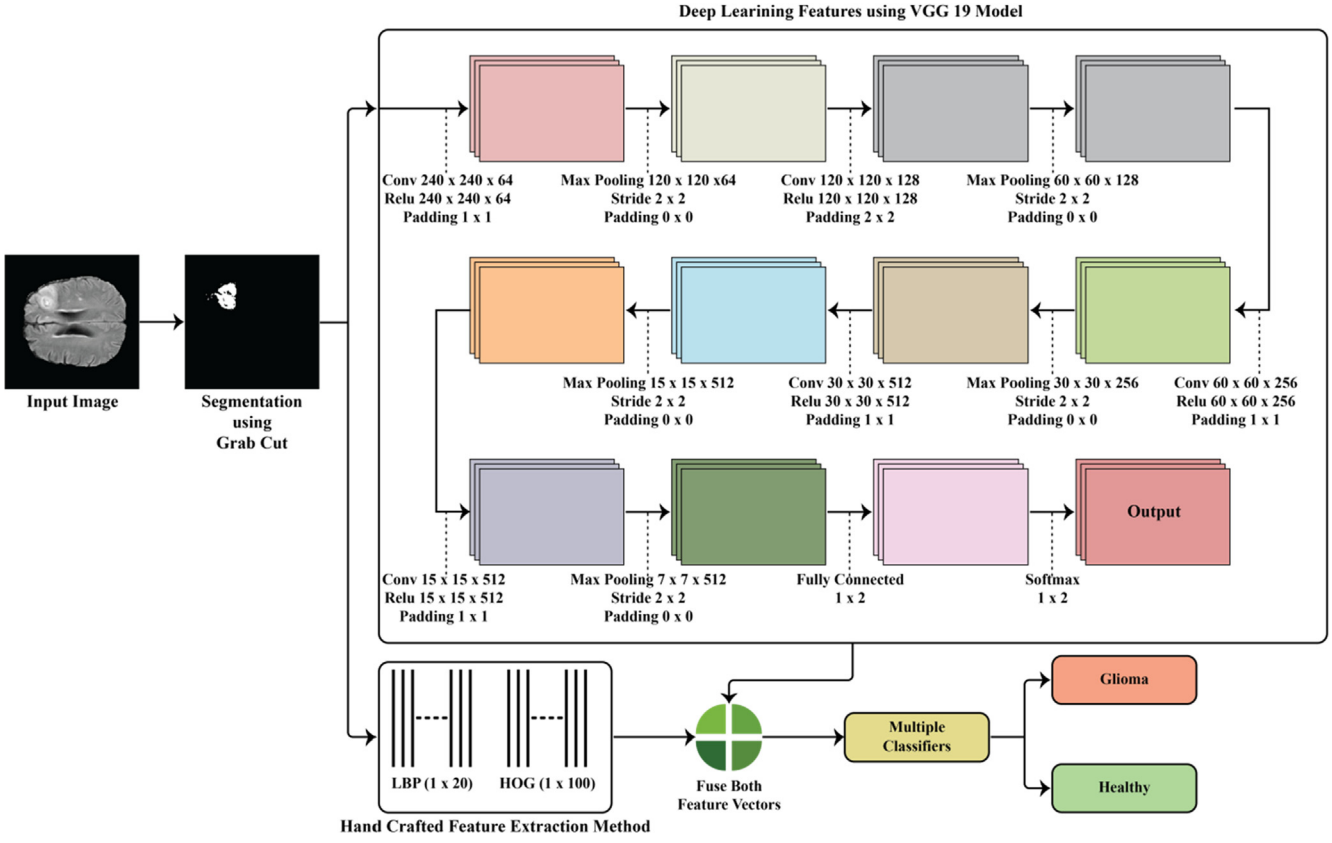

Fig. 1. Handcrafted and deep features fusion for brain tumor classification.

tion. At this stage, seed point is chosen on the basis of threshold between 0 and 180. The values of seed pints grow by adopting the neighboring pixel values in which the value of threshold is similar to primary seed point. As the iterations go on, identical pixels are grouped together and act as actual seed point. This process is repeated until similar pixel vales are grouped at a specified threshold level. The tumor segmented slices are shown in Fig. 2.

3.2. Training and testing using VGG 19

The proposed VGG 19 model consists of convolutional followed by max pooling and the fully connected layers. Each convolutional layer is utilized to perform feature mapping (activations) by convolving the input with linear filters bank. Learning is performed in training and followed through rectification layer in which non-linearity rectified

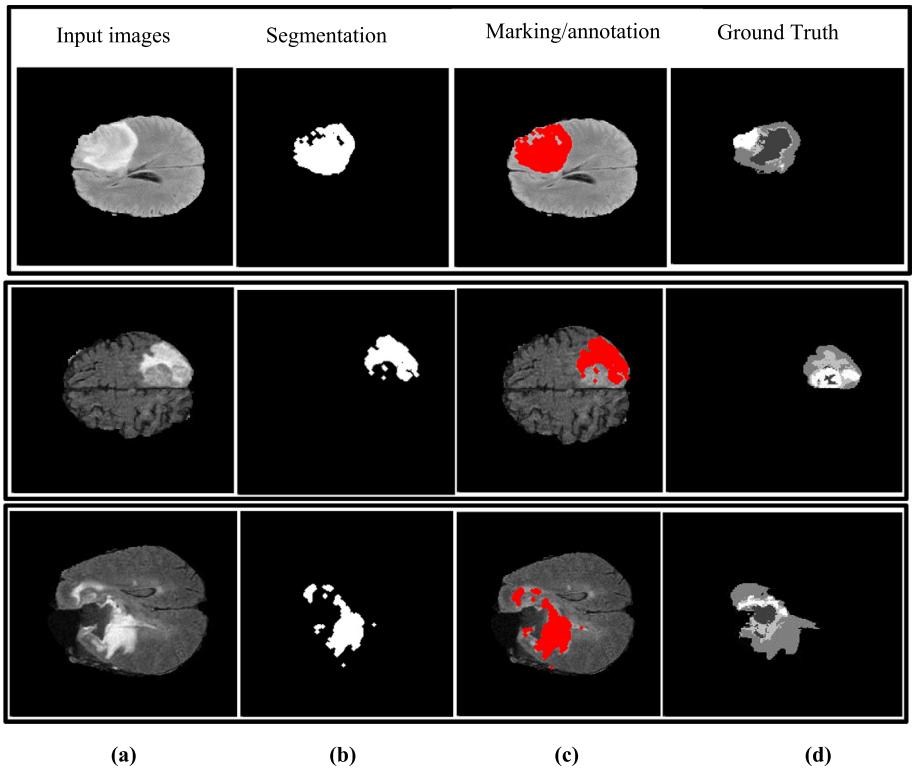

Fig. 2. Brain tumor segmented slices using proposed Grab cut algorithm (a) input images (b) segmented results (c) annotation (d) ground truth.

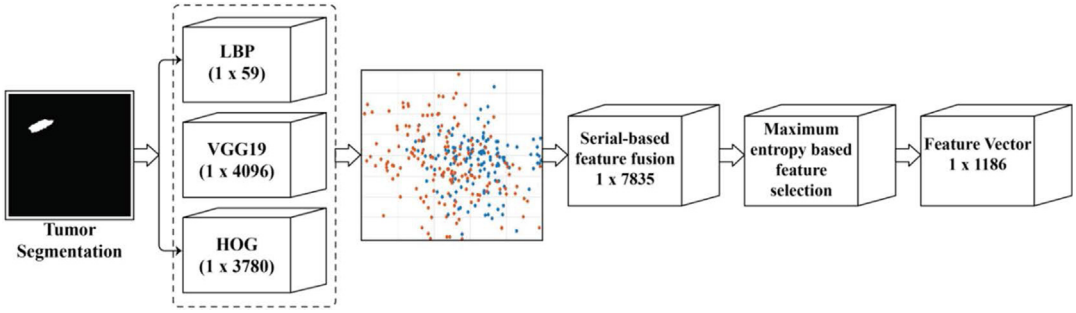

Fig. 3. Features fusion process.

linear unit (ReLU) is utilized on feature mapping. The feature mapping size of first convolutional layer is 240 whereas feature mapping on fully connected layer ($1\times1\times2$). This architecture encodes the feature hierarchy. The last fully connected layers are utilized to process features by linear operation that are followed through ReLU. The fully connected layer is 4096D vector as an output and last fully connected layer yields $1\times1\times2$ vector dimension that is supplied to the softmax layer (Raza et al., 2018) for the computation of posterior class probability.

3.3. Hand crafted feature extraction

In the proposed technique, hand crafted features i.e., LBP (Moulin, Liu, & Gray-Scale, 2002), HOG (Dalal & Triggs, 2005) and deep learning features are extracted to classify the gliomas and healthy images. The suggested approach is validated on fused features vector comprised of hand crafted and deep learning features. HOG features are widely utilized for object detection and are extracted across all grid dense locations from the image. The brain tumor shape and appearance might be characterized through intensity gradient using HOG features (1×3780) and LBP features (1×59).

3.3.1. Fusion of hand crafted and deep learning features

Data fusion is applied in several machine learning and computer vision applications. The features fusion is a vital task which combines more than one feature vectors. The presented approach is based on features fusion by entropy. The feature extraction and selection process is expressed in Fig. 3.

The three vectors are defined as:

$$f_{HOG1\times n} = \{HOG_{1\times1}, HOG_{1\times2}, HOG_{1\times3}, \cdots, HOG_{1\times n}\} \quad (1)$$

$$f_{VGG191\times m} = \{VGG19_{1\times1}, VGG19_{1\times2}, VGG19_{1\times3}, \cdots, VGG19_{1\times n}\} \quad (2)$$

$$f_{LBP1\times p} = \{LBP_{1\times1}, LBP_{1\times2}, LBP_{1\times3}, \cdots, LBP_{1\times n}\} \quad (3)$$

Moreover, extracted features are fused in a single vector.

$$\text{Fused(features vector)}_{1\times q} = \sum_{i=1}^{3}\{fHOG_{1\times n}, fVGG19_{1\times m}, fLBP_{1\times p} \quad (4)$$

where f is fused vector (1×1186). The entropy is applied on features vector for the selection of optimal features based on score. The feature selection process is mathematically explained in Eqs. (1)–(4). Entropy is used to select 1186 score-based features from 7835 features.

$$B_{He} = -NHe_b \sum_{i=1}^{n} p(f_i) \quad (5)$$

$$F_{select} = B_{He}(\max(f_i, 1186)) \quad (6)$$

In Eqs. (5) and (6), p represents features probability and He denotes entropy. The finally selected features are given to the classifiers in order to differentiate the glioma and healthy images.

3.4. Brain tumor classification

Segmented images are obtained using the proposed Grab cut algorithm. Then hand crafted and deep learning features are collected from all images. These images are supplied to multiple classifiers for example logistic regression (LGR) (Anderson, 2007), decision tree (DT) (Breiman, 1996), K nearest neighbor (KNN) (Breiman, 1996), ensemble (Amin, Sharif, Yasmin, Ali, & Fernandes, 2017), linear discriminant analysis (LDA) (Fisher, 1936) and SVM (Hastie, Tibshirani, & Friedman, 2008) for the classification. Comprehensive analysis is conducted for separating gliomas and healthy images.

3.5. Experimental setup

Three standard MRI benchmark datasets are used to evaluate the brain data (Kistler, Bonaretti, Pfahrer, Niklaus, & Büchler, 2013). BRATS 2015 is comprised of 220 HGG and 54 LGG included in training and 110 both HGG and LGG as testing cases. BRATS 2016 shares similar training database as BRATS 2015. BRATS 2017 contain 210 HGG and 75 LGG cases. The proposed technique experiments are made on Intel Core I7 3.4 GHz, RAM 16.0 GB, 64 bit operating system (OS), x64 based processor with NIVIDIA GeForce GTX 1080 GPU on MATLAB 2018b. The datasets description is stated in Table 2.

Table 2
Description of datasets used in proposed method (0.5 hold out cross validation is used where half images are utilized for training and half for testing).

Datasets	Sequences	Cases/volume	Dimension	High and low grade images	Normal and Glioma images (Approx.)
BRATS 2015 Challenge	Flair, T1, T1c and T2	54 LGG, 220 HGG in training and 110 both HGG and LGG in testing	$240 \times 240 \times 155 \times 4$ (155 slices in each case) 4 denotes number of sequences	33,480 LGG images, 136,400 HGG images in training and 68,200 both HGG and LGG images in testing	15,456 non-glioma and 16,564 glioma images in training and 16,544 glioma and 7636 non-glioma images in testing
BRATS 2017 Challenge		75 LGG, 210 HGG cases		46,500 LGG images, 130,200 HGG images	19,032 non-glioma and 15,272 glioma images
BRATS 2016 Challenge	54 LGG, 220 HGG are included in training and testing cases are not given.				

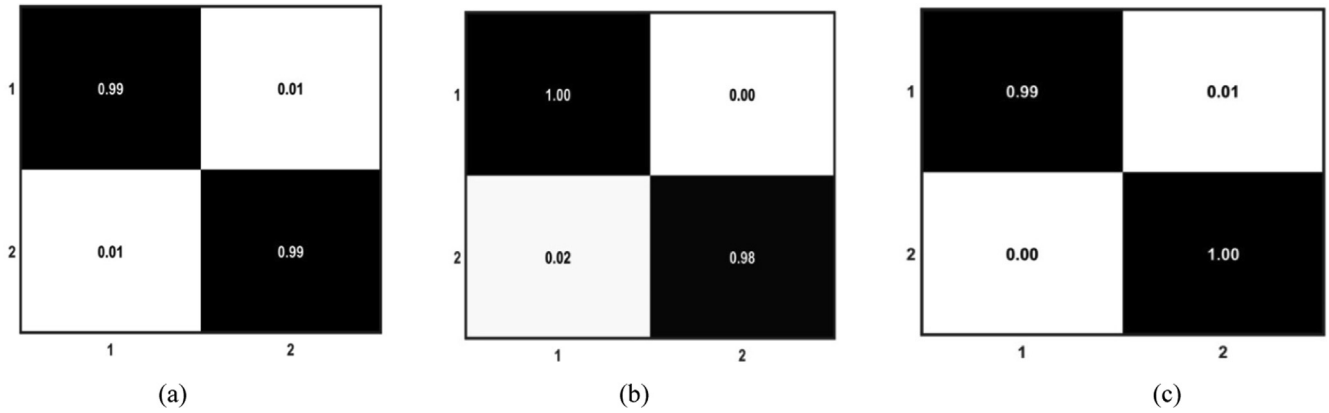

Fig. 4. Confusion matrix (a) HOG + LBP (b) Deep features (c) Features fusion.

Table 3
Results of tumor and non-tumor slices on BRATS 2015.

Multiple classifiers	HOG + LBP					Deep features					Fusion of HOG + LBP + Deep features				
	Accuracy	SPE	SEN	DSC	Jaccard	Accuracy	SPE	SEN	DSC	Jaccard	Accuracy	SPE	SEN	DSC	Jaccard
DT	0.9598	0.9582	0.9619	0.9538	0.9116	0.9813	0.9854	0.9607	0.9448	0.8953	***0.9963***	***1.000***	***0.9955***	***0.9977***	***0.9955***
LGR	0.9543	0.9578	0.9498	0.9478	0.9008	0.8519	0.9853	0.5406	0.6865	0.5227	***0.9977***	***0.9892***	***0.9994***	***0.9986***	***0.9972***
KNN	0.9948	0.9945	0.9949	0.9969	0.9938	0.8903	0.9812	0.6236	0.7429	0.5909	***0.9982***	***1.000***	***0.9959***	***0.9979***	***0.9959***
Ensemble	0.9967	0.9945	0.9972	0.9980	0.9960	0.9606	0.9784	0.8777	0.8871	0.7971	***0.9890***	***0.9934***	***0.9835***	***0.9876***	***0.9754***
LDA	0.9934	0.9944	0.9932	0.9960	0.9921	0.9822	0.9821	0.9825	0.9465	0.8984	***0.9945***	***0.9967***	***0.9917***	***0.9938***	***0.9876***
SVM	0.9981	1.000	0.9977	0.9989	0.9977	0.9878	0.9866	0.9942	0.9636	0.9297	***0.9909***	***0.9903***	***0.9916***	***0.9896***	***0.9793***

Table 4
Results of tumor and non-tumor slices on 2016.

Multiple classifiers	HOG + LBP					Deep features					Fusion of HOG + LBP + Deep features				
	Accuracy	SPE	SEN	DSC	Jaccard	Accuracy	SPE	SEN	DSC	Jaccard	Accuracy	SPE	SEN	DSC	Jaccard
DT	0.9757	0.9835	0.9660	0.9726	0.9467	0.9616	0.9704	0.9506	0.9565	0.9167	***0.9954***	***0.9984***	***0.9917***	***0.9948***	***0.9897***
LGR	0.9329	0.9821	0.8812	0.9276	0.8650	0.9634	0.9799	0.9435	0.9590	0.9213	***0.9982***	***1.000***	***0.9959***	***0.9979***	***0.9959***
KNN	0.9238	0.9441	0.8993	0.9147	0.8428	0.9909	0.9903	0.9916	0.9896	0.9793	***0.9973***	***0.9984***	***0.9959***	***0.9969***	***0.9938***
Ensemble	0.9982	0.9967	1.000	0.9979	0.9959	0.9927	0.9935	0.9917	0.9917	0.9835	***1.000***	***1.000***	***1.000***	***1.000***	***1.000***
LDA	0.9756	0.9783	0.9722	0.9722	0.9459	0.9835	0.9934	0.9714	0.9814	0.9636	***0.9963***	***0.9967***	***0.9958***	***0.9958***	***0.9917***
SVM	0.9901	0.9942	0.9848	0.9886	0.9774	0.9963	1.000	0.9917	0.9959	0.9917	***0.9945***	***0.9935***	***0.9958***	***0.9938***	***0.9876***

Table 5
Classification results (tumor and non-tumor slices) on BRATS 2017.

Multiple classifiers	HOG + LBP					Deep features					Fusion of HOG + LBP + Deep features				
	Accuracy	SPE	SEN	DSC	Jaccard	Accuracy	SPE	SEN	DSC	Jaccard	Accuracy	SPE	SEN	DSC	Jaccard
DT	0.9784	0.9821	0.9600	0.9359	0.8796	0.9609	0.9608	0.9610	0.9552	0.9143	***0.9927***	***0.9937***	***0.9919***	***0.9935***	***0.9871***
LGR	0.9897	0.9888	0.9943	0.9694	0.9405	0.9205	0.9489	0.8876	0.9120	0.8382	***0.9973***	***0.9959***	***0.9984***	***0.9976***	***0.9951***
KNN	0.9916	0.9932	0.9834	0.9753	0.9519	0.8905	0.9369	0.8410	0.8814	0.7879	***0.9963***	***0.9958***	***0.9967***	***0.9967***	***0.9935***
Ensemble	0.9831	0.9832	0.9826	0.9494	0.9037	0.9832	0.9839	0.9823	0.9809	0.9624	***0.9982***	***0.9959***	***1.000***	***0.9984***	***0.9967***
LDA	0.9925	0.9944	0.9835	0.9781	0.9572	0.9981	1.000	0.9977	0.9989	0.9977	***0.9945***	***0.9958***	***0.9935***	***0.9951***	***0.9903***
SVM	0.9944	0.9955	0.9890	0.9836	0.9677	0.9967	0.9945	0.9972	0.9980	0.9960	***0.9954***	***0.9958***	***0.9951***	***0.9959***	***0.9919***

4. Results and discussion

The confusion matrix classes (1 for healthy and 2 for glioma) are depicted in Fig. 4. The results are evaluated on individual and fused features vector independently for tumor classification shown in Tables 3–5.

The SVM classifier obtains 0.9909 Accuracy on BRATS 2015 using fusion vector, 0.9909 Accuracy using HOG + LBP features vector and 0.9866 Accuracy on deep learning features (see Table 3). The LGR classifier demonstrates maximum 0.9982 Accuracy on fused features vector, 0.9329 on HOG + LBP features vector and 0.9634 Accuracy on deep features vector (see Table 4). The ensemble classifier achieves maximum 0.9982 Accuracy on fused features vector, 0.9831 Accuracy on HOG + LBP features vector and 0.9832 Accuracy on deep features vector (see Table 5). The classification between high and low grade tumor is mentioned in Tables 6–8.

On BRATS 2017, LGR classifier performs better to distinguish between high and low grade glioma with 0.9925 Accuracy while SVM achieves 0.9359 Accuracy (see Table 6). On BRATS 2015, Ensemble obtains highest 0.9130 Accuracy whereas minimum 0.8143 Accuracy is shown on LDA (see Table 7). On BRATS 2016, highest 0.9174 Accuracy is obtained using Ensemble classifier and minimum 0.7726 Accuracy is achieved using SVM classifier (see Table 8). The receiver operating characteristic (ROC) curve of proposed features vector is shown in Fig. 5.

Table 6
Classification results (high grade and low grade slices) on BRATS 2017.

Multiple classifiers	HOG + LBP					Deep features					Fusion of (HOG + LBP + Deep features)				
	Accuracy	SPE	SEN	DSC	Jaccard	Accuracy	SPE	SEN	DSC	Jaccard	Accuracy	SPE	SEN	DSC	Jaccard
DT	0.9774	0.9864	0.9889	0.9570	0.9780	0.9774	0.9843	0.9915	0.9906	0.9672	***0.9871***	***0.9840***	***0.9672***	***0.9711***	***0.9440***
LGR	0.9677	0.9860	0.9271	0.8990	0.9468	0.9880	0.9894	0.9916	0.9833	0.9754	***0.9925***	***0.9946***	***0.9905***	***0.9929***	***0.9859***
KNN	0.9774	0.9862	0.9570	0.9271	0.9622	0.9903	0.9843	0.9916	0.9876	0.9672	***0.9774***	***0.9840***	***0.9672***	***0.9712***	***0.9440***
Ensemble	0.9771	0.9864	0.9889	0.9570	0.9780	0.9871	0.9893	0.9674	0.9833	0.9520	***0.9839***	***0.9791***	***0.9915***	***0.9790***	***0.9590***
LDA	0.9871	0.9864	0.9889	0.9570	0.9780	0.9839	0.9840	0.9672	0.9754	0.9440	***0.9806***	***0.9893***	***0.9674***	***0.9754***	***0.9520***
SVM	0.9359	0.8426	0.8426	0.8198	0.9010	0.9935	0.9840	0.9672	0.9712	0.9440	***0.9871***	***0.9946***	***0.9756***	***0.9836***	***0.9677***

Table 7
Classification results (high grade and low grade slices) on BRATS 2015.

Multiple classifiers	HOG + LBP					Deep features					Fusion of (HOG + LBP + Deep features)				
	Accuracy	SPE	SEN	DSC	Jaccard	Accuracy	SPE	SEN	DSC	Jaccard	Accuracy	SPE	SEN	DSC	Jaccard
DT	0.8530	0.8206	0.8776	0.8716	0.7725	0.8522	0.7881	0.9008	0.8741	0.7763	***0.8788***	***0.8451***	***0.9021***	***0.8980***	***0.8149***
LGR	0.8356	0.8206	0.8469	0.8542	0.7455	0.8373	0.7332	0.9160	0.8650	0.7622	***0.8723***	***0.8161***	***0.9150***	***0.8907***	***0.8030***
KNN	0.8917	0.8700	0.9082	0.9051	0.8266	0.8926	0.8632	0.9146	0.9068	0.8294	***0.9014***	***0.9058***	***0.8980***	***0.9119***	***0.8381***
Ensemble	0.8356	0.7758	0.8810	0.8590	0.7529	0.8449	0.7113	0.9466	0.8739	0.7761	***0.9130***	***0.8834***	***0.9354***	***0.9244***	***0.8594***
LDA	0.8143	0.8655	0.7755	0.8261	0.7037	0.8402	0.7141	0.9355	0.8695	0.7692	***0.8569***	***0.7265***	***0.9558***	***0.8836***	***0.7915***
SVM	0.8414	0.8072	0.8673	0.8615	0.7567	0.8392	0.7085	0.9381	0.8692	0.7686	***0.8820***	***0.8386***	***0.9150***	***0.8982***	***0.8152***

Table 8
Classification results (high grade and low grade slices) on BRATS 2016.

Multiple classifiers	HOG + LBP					Deep features					Fusion of (HOG + LBP + Deep features)				
	Accuracy	SPE	SEN	DSC	Jaccard	Accuracy	SPE	SEN	DSC	Jaccard	Accuracy	SPE	SEN	DSC	Jaccard
DT	0.8769	0.8565	0.8923	0.8919	0.8049	0.8532	0.7747	0.9126	0.8762	0.7797	***0.8880***	***0.8475***	***0.9186***	***0.9033***	***0.8236***
LGR	0.8522	0.8531	0.8516	0.8678	0.7664	0.8373	0.7309	0.9177	0.8653	0.7625	***0.8537***	***0.7993***	***0.8948***	***0.8744***	***0.7769***
KNN	0.9092	0.8789	0.9321	0.9212	0.8539	0.8759	0.8430	0.9008	0.8921	0.8052	***0.8698***	***0.7953***	***0.9313***	***0.8869***	***0.7968***
Ensemble	0.8643	0.8262	0.8931	0.8823	0.7894	0.8387	0.7152	0.9321	0.8681	0.7669	***0.9174***	***0.8733***	***0.9508***	***0.9291***	***0.8676***
LDA	0.8276	0.8935	0.7778	0.8371	0.7198	0.8402	0.7152	0.9347	0.8694	0.7690	***0.8353***	***0.7007***	***0.9372***	***0.8663***	***0.7642***
SVM	0.7726	0.8610	0.7057	0.7794	0.6385	0.8392	0.7063	0.9398	0.8694	0.7689	***0.8614***	***0.8206***	***0.8923***	***0.8800***	***0.7857***

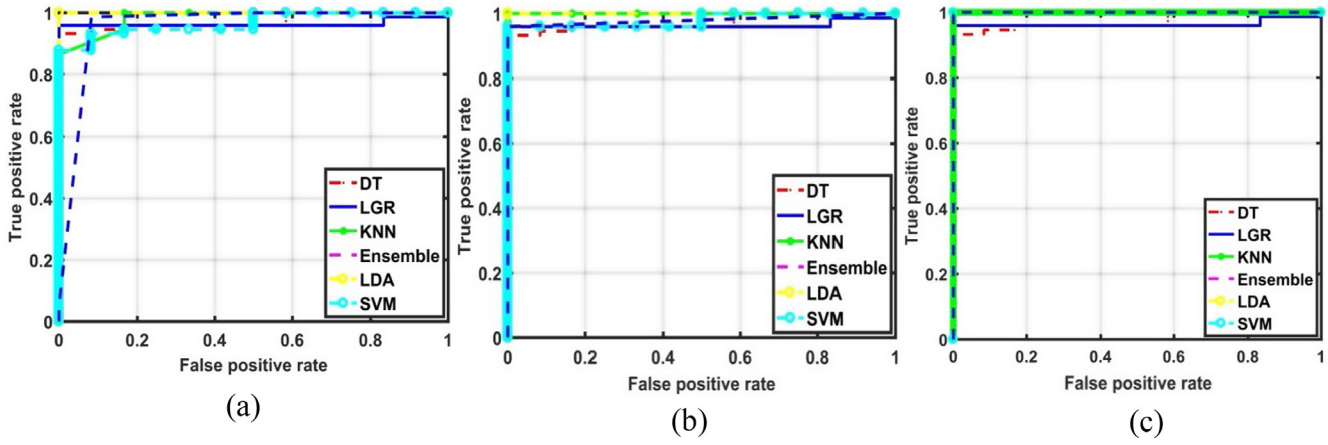

Fig. 5. ROC (a) HOG + LBP (b) Deep features (c) Features fusion.

Table 9
Computational times of proposed method.

Steps	Computational time
HOG and LBP features	21.315597 s
Deep features	30.1664 s
Features fusion	4.9023 s
Testing	24.2222 s

In these experiments, HOG, LBP, deep features (VGG-19) as well as fusion of HOG, LBP and deep features are supplied to different classifiers for classification. In this scenario, it is observed that fused features vector performs better as compared to individual deep and hand crafted features (HOG, LBP). The proposed method running time is mentioned in Table 9. The comparison of suggested method is given in Table 10.

The suggested approach is contrasted with existing state of art approaches to reveal that presented method supersedes the existing methods.

5. Conclusion

The hand crafted and deep learning features are acquired from the segmented images; these are optimized through the entropy. The optimized features are fused with the help of serial fusion approach to create a single features vector. Finally, the classification is performed with various classifiers to predict the glioma or healthy images. The proposed method is individually trained and tested on various benchmark databases such as BRATS 2015–17. The maximum testing results depict Accuracy = 0.9878 and DSC = 0.9636 on BRATS 2015. On BRATS 2016, Accuracy = 0.9963 and DSC = 0.9959 and on BRATS 2017, Accuracy = 0.9967 and DSC = 0.9980 are achieved. The satisfactory results depict presented approach strength.

Table 10
Proposed method comparison with existing approaches.

BRATS Datasets	Methods	DSC	SEN
2015	CNN (Pereira et al., 2016)	0.78	–
	Deep CNN (Havaei, 2017)	0.84	0.87
	Deep Medic + CRF (Kamnitsas, 2017)	0.90	0.90
	Input Cascaded CNN (Larochelle & Jodoin, 2015)	0.88	0.87
	Proposed	**0.99**	**0.99**
2016	Iterative random forest (Ellwaa, 2016)	0.81 ± 0.09	0.84 ± 0.10
	Proposed	**1.00**	**1.00**
2017	Fully CNN (Van Der Kouwe, 2017)	0.83	–
	U-Net (Amorim et al., 2017)	0.63	0.99
	Recurrent neural networks (Simon Andermatt & Cattin, 2017)	0.86	0.81
	Proposed	**0.99**	**0.99**

Acknowledgement

This work was supported by the research Project [A Framework for Detection and Classification of Brain Tumor on the Early Onset]; Prince Sultan University; Saudi Arabia [SSP-18-5-02]. Additionally, this work was partially supported by the Artificial Intelligence and Data Analytics (AIDA) Lab, Prince Sultan University, Riyadh, Saudi Arabia.

References

Abd-Ellah, M. K., Awad, A. I., Khalaf, A. A., & Hamed, H. F. (2018). Two-phase multi-model automatic brain tumour diagnosis system from magnetic resonance images using convolutional neural networks. *EURASIP Journal on Image and Video Processing, 2018*(1), 97.

Anderson, R. (2007). The Credit Scoring Toolkit. Oxford University Press.

Amin, J., Sharif, M., Raza, M., & Yasmin, M. (2018). Detection of brain tumor based on features fusion and machine learning. *Journal of Ambient Intelligence and Humanized Computing*, 1–17.

Amin, J., Sharif, M., Yasmin, M., Ali, H., & Fernandes, S. L. (2017). A method for the detection and classification of diabetic retinopathy using structural predictors of bright lesions. *Journal of Computational Science, 19*, 153–164.

Amin, J., Sharif, M., Yasmin, M., & Fernandes, S. L. (2017). A distinctive approach in brain tumor detection and classification using MRI. *Pattern Recognition Letters*.

Amin, J., Sharif, M., Yasmin, M., & Fernandes, S. L. (2018). Big data analysis for brain tumor detection: Deep convolutional neural networks. *Future Generation Computer Systems, 87*, 290–297.

Amorim, P. H. A. C., Escudero, V. S., Oliveira, G. G., Pereira, D. D. C., Santos, S. M., & Scussel, A. A. H. M. (2017). 3D U-nets for brain tumor segmentation in MICCAI 2017 BraTS challenge. *Proceedings of the 6th MICCAI BraTS Challenge (2017)*. .

Ansari, G. J., Shah, J. H., Yasmin, M., Sharif, M., & Fernandes, S. L. (2018). A novel machine learning approach for scene text extraction. *Future Generation Computer Systems, 87*, 328–340.

Bauer, S., Fejes, T., Slotboom, J., Wiest, R., Nolte, L.-P., & Reyes, M. (2012). Segmentation of brain tumor images based on integrated hierarchical classification and regularization. *MICCAI BraTS workshop*. Nice: Miccai Society.

Bauer, S., Nolte, L.-P., & Reyes, M. (2011). Fully automatic segmentation of brain tumor images using support vector machine classification in combination with hierarchical conditional random field regularization. In *International conference on medical image computing and computer-assisted intervention* (pp. 354–361). Springer.

Breiman, L. (1996). Bagging Predictors. *Machine Learning, 26*, 123–140.

Chen, S., Ding, C., & Liu, M. (2019). Dual-force convolutional neural networks for accurate brain tumor segmentation. *Pattern Recognition, 88*, 90–100.

Dalal, N., & Triggs, B. (2005). Histograms of Oriented Gradients for Human Detection. *IEEE Computer Society Conference on Computer Vision and Pattern Recognition, 1*, 886–893.

Dong, H., Yang, G., Liu, F., Mo, Y., & Guo, Y. (2017). Automatic brain tumor detection and segmentation using U-Net based fully convolutional networks. In *Annual conference on medical image understanding and analysis* (pp. 506–517). Springer.

Dvořák, P., & Menze, B. (2015). Local structure prediction with convolutional neural networks for multimodal brain tumor segmentation. In *International MICCAI workshop on medical computer vision* (pp. 59–71). Springer.

Ellwaa, A. et al. (2016). Brain tumor segmantation using random forest trained on iteratively selected patients. In *International workshop on brainlesion: Glioma, multiple sclerosis, stroke and traumatic brain injuries* (pp. 129–137). Springer.

Fisher, R. A. (1936). The Use of Multiple Measurements in Taxonomic Problems. *Annals of Eugenics, 7*, 179–188. Available at https://digital.library.adelaide.edu.au/dspace/handle/2440/15227.

Geremia, E., Menze, B. H., Clatz, O., Konukoglu, E., Criminisi, A., & Ayache, N. (2010). Spatial decision forests for MS lesion segmentation in multi-channel MR images. In *International conference on medical image computing and computer-assisted intervention* (pp. 111–118). Springer.

Goetz, M., Weber, C., Bloecher, J., Stieltjes, B., Meinzer, H.-P., & Maier-Hein, K. (2014). Extremely randomized trees based brain tumor segmentation. In *Proceeding of BRATS challenge-MICCAI* (pp. 006–011).

Havaei, M. et al. (2017). Brain tumor segmentation with deep neural networks. *Medical Image Analysis, 35*, 18–31.

Havaei, M., Dutil, F., Pal, C., Larochelle, H., & Jodoin, P.-M. (2015). A convolutional neural network approach to brain tumor segmentation. In *BrainLes 2015* (pp. 195–208). Springer.

https://medium.com/@sidereal/cnns-architectures-lenet-alexnet-vgg-goo-glenet-resnet-and-more-666091488df5, accessed by 7/4/2019.

Hastie, T., Tibshirani, R., & Friedman, J. (2008). The Elements of Statistical Learning (second edition). New York: Springer.

Huang, M., Yang, W., Wu, Y., Jiang, J., Chen, W., & Feng, Q. (2014). Brain tumor segmentation based on local independent projection-based classification. *IEEE Transactions on Biomedical Engineering, 61*(10), 2633–2645.

Hussain, S., Anwar, S. M., & Majid, M. (2018). Segmentation of glioma tumors in brain using deep convolutional neural network. *Neurocomputing, 282*, 248–261.

Kamnitsas, K. et al. (2017). Efficient multi-scale 3D CNN with fully connected CRF for accurate brain lesion segmentation. *Medical Image Analysis, 36*, 61–78.

Kistler, M., Bonaretti, S., Pfahrer, M., Niklaus, R., & Büchler, P. (2013). The virtual skeleton database: An open access repository for biomedical research and collaboration. *Journal of Medical Internet Research, 15*(11), e245.

Kleesiek, J., Biller, A., Urban, G., Kothe, U., Bendszus, M., & Hamprecht, F. (2014). Ilastik for multi-modal brain tumor segmentation. *Proceedings MICCAI BraTS (Brain Tumor Segmentation Challenge)*, 12–17.

Kwon, D., Shinohara, R. T., Akbari, H., & Davatzikos, C. (2014). Combining generative models for multifocal glioma segmentation and registration. In *International conference on medical image computing and computer-assisted intervention* (pp. 763–770). Springer.

Larochelle, H., & Jodoin, P.-M. (2015). A convolutional neural network approach to brain tumor segmentation. In *Brainlesion: Glioma, multiple sclerosis, stroke and traumatic brain injuries: First international workshop, brainles 2015, held in conjunction with MICCAI 2015, Munich, Germany, October 5, 2015, revised selected papers* (pp. 195). Springer.

Liaqat, A., Khan, M. A., Shah, J. H., Sharif, M., Yasmin, M., & Fernandes, S. L. (2018). Automated ulcer and bleeding classification from WCE images using multiple features fusion and selection. *Journal of Mechanics in Medicine and Biology, 18*(04), 1850038.

Litjens, G. et al. (2017). A survey on deep learning in medical image analysis. *Medical Image Analysis, 42*, 60–88.

Mahmud, M., Kaiser, M. S., Hussain, A., & Vassanelli, S. (2018). Applications of deep learning and reinforcement learning to biological data. *IEEE Transactions on Neural Networks and Learning Systems, 29*(6), 2063–2079.

Menze, B. H. et al. (2014). The multimodal brain tumor image segmentation benchmark (BRATS). *IEEE Transactions on Medical Imaging, 34*(10), 1993–2024.

Mitra, J. et al. (2014). Lesion segmentation from multimodal MRI using random forest following ischemic stroke. *NeuroImage, 98*, 324–335.

Moulin, P., Liu, J., & Gray-Scale, M. (2002). Rotation Invariant Texture Classification with Local Binary Patterns. *IEEE Transactions on Pattern Analysis and Machine Intelligence, Mag, 24,* 971–987.

Naqi, S., Sharif, M., Yasmin, M., & Fernandes, S. L. (2018). Lung nodule detection using polygon approximation and hybrid features from CT images. *Current Medical Imaging Reviews, 14*(1), 108–117.

Nida, N., Sharif, M., Khan, M. U. G., Yasmin, M., & Fernandes, S. L. (2016). A framework for automatic colorization of medical imaging. *IIOAB J, 7*, 202–209.

Pereira, S., Pinto, A., Alves, V., & Silva, C. A. (2015). Deep convolutional neural networks for the segmentation of gliomas in multi-sequence MRI. In *BrainLes 2015* (pp. 131–143). Springer.

Pereira, S., Pinto, A., Alves, V., & Silva, C. A. (2016). Brain tumor segmentation using convolutional neural networks in MRI images. *IEEE Transactions on Medical Imaging, 35*(5), 1240–1251.

Rao, A., Ledig, C., Newcombe, V., Menon, D., & Rueckert, D. (2014). Contusion segmentation from subjects with traumatic brain injury: A random forest framework. In *2014 IEEE 11th international symposium on biomedical imaging (ISBI)* (pp. 333–336). IEEE.

Raza, M., Sharif, M., Yasmin, M., Khan, M. A., Saba, T., & Fernandes, S. L. (2018). Appearance based pedestrians' gender recognition by employing stacked auto encoders in deep learning. *Future Generation Computer Systems, 88*, 28–39.

Reza, S. M., Mays, R., & Iftekharuddin, K. M. (2015). Multi-fractal detrended texture feature for brain tumor classification. In *Medical imaging 2015: Computer-aided diagnosis* (pp. 941410). International Society for Optics and Photonics.

Shah, J. H., Sharif, M., Yasmin, M., & Fernandes, S. L. (2017). Facial expressions classification and false label reduction using LDA and threefold SVM. *Pattern Recognition Letters*.

Sharif, M., Khan, M. A., Faisal, M., Yasmin, M., & Fernandes, S. L. (2018). A framework for offline signature verification system: Best features selection approach. *Pattern Recognition Letters*.

Simon Andermatt, S. P., & Cattin, Philippe (2017). Multi-dimensional gated recurrent units for brain tumor segmentation. *Proceedings of the 6th MICCAI BraTS challenge (2017)*. .

Strangman, D. (2009). Clinical practice guidelines for the management of adult gliomas: Astrocytomas and oligodendrogliomas. *Cancer Council Australia/Australian Cancer Network/Clinical Oncological Society of Australia*.

Thompson, G., Mills, S., Coope, D., O'connor, J., & Jackson, A. (2011). Imaging biomarkers of angiogenesis and the microvascular environment in cerebral tumours. *The British Journal of Radiology, 84* (special_issue_2), S127–S144.

Tustison, N. J. et al. (2015). Optimal symmetric multimodal templates and concatenated random forests for supervised brain tumor segmentation (simplified) with ANTsR. *Neuroinformatics, 13*(2), 209–225.

Van Der Kouwe, A. (2017). Brain tumor segmentation from multi modal MR images using fully convolutional neural network. *Proceedings of the 6th MICCAI BraTS challenge*. .

Van Leemput, K., Maes, F., Vandermeulen, D., & Suetens, P. (1999). Automated model-based tissue classification of MR images of the brain. *IEEE Transactions on Medical Imaging, 18*(10), 897–908.

Wu, W., Chen, A. Y., Zhao, L., & Corso, J. J. (2014). Brain tumor detection and segmentation in a CRF (conditional random fields) framework with pixel-pairwise affinity and superpixel-level features. *International Journal of Computer Assisted Radiology and Surgery, 9*(2), 241–253.

Zhao, X., Wu, Y., Song, G., Li, Z., Zhang, Y., & Fan, Y. (2018). A deep learning model integrating FCNNs and CRFs for brain tumor segmentation. *Medical Image Analysis, 43*, 98–111.

Zikic, D., Ioannou, Y., Brown, M., & Criminisi, A. (2014). Segmentation of brain tumor tissues with convolutional neural networks. *Proceedings MICCAI-BRATS*, 36–39.